A MODIFIED VERSION OF THE MOSAIC PHASE GRADIENT AUTOFOCUS

Stefan Leier, Martin Kronig and Abdelhak M. Zoubir

Signal Processing Group
Technische Universität Darmstadt
{leier, kronig, zoubir}@spg.tu-darmstadt.de

ABSTRACT

High resolution radar and sonar images can be constructed using either spotlight or stripmap synthetic aperture systems. In the presence of residual phase errors, the respective images are blurred and their quality degrades dramatically. Typically, autofocus techniques are applied in spotlight operation to correct the degradation. However, for stripmap modes, the use of autofocus methods is not straightforward due to a spatially variant point spread function. We propose modifications to the existing mosaic phase gradient algorithm to overcome its drawbacks and to make it more applicable for stripmap synthetic aperture systems.

Index Terms— stripmap, synthetic aperture techniques, autofocus techniques, mosaic phase gradient autofocus

1. INTRODUCTION

Synthetic aperture imaging is a technique to produce high-resolution imagery by constantly transmitting pulses while moving a sensor along a trajectory. Thus, an aperture is synthesized whose length automatically adjusts itself to a range of interest. This inherently overcomes the drawbacks of conventional imaging techniques, namely the loss in along-track resolution for increasing range values. However, imprecise knowledge of the exact sensor location at each transmission and reception time causes blurred imagery.

The objective of autofocus techniques is to enhance the quality of the degraded synthetic aperture image. They can be divided into two groups, depending on the two common operating modes of synthetic aperture systems, namely stripmap and spotlight [1]. For the latter, the well-known Phase Gradient Autofocus (PGA) [2] algorithm attains nearly a diffraction limited restoration of degraded images by compensating residual phase errors due to unknown path deviations. It is directly applied to the defocused image, and thus, computationally convenient. Its applicability has been proven for a wide-variety of scenes in synthetic aperture radar (SAR). However, it has some limiting restrictions in its standard version, e.g. the point spread function (PSF) has to be identical for each point in the image, which is only met in spotlight

mode. The authors of [2] introduced the Phase Curvature Autofocus (PCA) as an attempt to extend the PGA to work for stripmap synthetic apertures in [3]. For stripmap imaging, the phase history of collected data is limited by the beamwidth of the physical aperture capturing only a fraction of the image. Thus, the PSF is spatially variant and the spotlight approximations do not hold anymore. The PCA assumes a narrow-band system to overcome the range dependency and reduces the underlying blurring model to 1-D discarding the 2-D character of the stripmap blurring function [3, 4]. Therefore, it is rarely used, especially for sonar applications, where mostly wide-band signals occur. The Stripmap Phase Gradient Autofocus (SPGA) algorithm was introduced in [5] to work with less approximations. However, rather than focusing the blurred image directly by applying an iterative phase correction in the wavenumber domain, as do the PGA and PCA, it estimates the path deviations of the imaging platform. Afterwards, it uses the estimated platform path to reconstruct a new focused image using appropriate synthetic aperture imaging techniques. This procedure requires several iterations to obtain a well-focused image which leads to a high computational complexity.

A different approach is introduced in [6], called the mosaic Phase Gradient Autofocus (mPGA). Here, the standard PGA is applied to stripmap synthetic aperture sonar (SAS) imagery by dividing the entire image into overlapping along-track segments, which are then treated as spotlight images. Each stripe is processed individually by the PGA and then re-assembled. While the mPGA overcomes the range dependency of stripmap phase errors and is computationally attractive, it does not consider targets at different along-track locations and, therefore, neglects their varying error information. This may lead to an emphasis in the focusing of prominent scatterers, while remaining scatterers of the same stripe are even more defocused. Additionally, the individual stripe processing may cause a linear misalignment during the stitching process of the along-track segments.

In this paper, we propose a modified version of the mPGA to alleviate its shortcomings. We account for the along-track dependency of the motion error by dividing the entire image into true mosaics, i.e. introducing 2-D sub-images. Moreover, we overcome the linear shift problem, which is induced

by occurring linear phase errors in the phase estimation of the PGA, by co-registration of the individual sub-images before and after each iteration of the autofocusing technique. The validity of the new approach is demonstrated using simulations on synthetic data and a full-reference image quality method.

2. SYNTHETIC APERTURE DATA MODEL

Consider a set of D stationary point scatterers located at positions $[x_d, y_d]^T$, $d = 1, \ldots, D$, with reflectivity σ_d. The ideal target scene [1] can be described as

$$f(x, y) = \sum_{d=1}^{D} \sigma_d \delta \left(x + X_c - x_d, y - y_d \right),$$

$$\text{for } y \in [-Y_0, Y_0] \text{ and } x \in [-X_0, X_0]$$

(1)

where Y_0 and X_0 are the boundaries in along-track, y, and range, x, direction, respectively. Moreover, X_c describes the standoff distance to the center point of the target scene and $\delta(x, y)$ is the two-dimensional delta function. The convolution between transmitted impulse, $p(t)$, and the ideal target scene $f(x, y)$ of (1) yields the received synthetic aperture echo data of a mono-static configuration as

$$e(u, t) = \sum_{d=1}^{D} \sigma_d \cdot p \left(t - \tau_d(u) \right).$$

(2)

In (2), the round-trip delay between the transceiver of the mono-static configuration located at position $[0, u]^T$ and the dth target is given by

$$\tau_d(u) = \frac{2}{c} \sqrt{x_d^2 + (y_d - u)^2}.$$

(3)

After demodulation and analog to digital conversion, an estimate $\hat{f}(x_n, y_m)$, $n = 1, \ldots, N_x$ and $m = 1, \ldots, N_y$, of the target reflectivity function is obtained by applying a synthetic aperture imaging algorithm, for example time-domain backprojection [1]. We represent the image reconstruction technique as a mapping function between the discrete echo signals, $e(u_i, t_j)$, with $i = 1, \ldots, M_u$ and $j = 1, \ldots, M_t$ and the discretized target grid area as

$$\hat{f}(x_n, y_m) = \mathcal{I} \left\{ e(u_i, t_j) \right\},$$

(4)

where M_u and M_t are the number of slow-time positions and fast-time samples, respectively.

2.1. Motion Error Model

The advantages of synthetic apertures come along with the prerequisite of sub-wavelength accuracy of sensor positions. Otherwise, phase errors are induced causing image degradation. Of all degrees of freedom of movement, the unknown

displacement in range direction or sway, $x_e(u)$, is the most severe. It leads to a significant mismatch between the assumed echo delay of (3) and the true but unknown round-trip delay

$$\tilde{\tau}_d(u) = \frac{2}{c} \sqrt{(x_d - x_e(u))^2 + (y_d - u)^2}.$$

(5)

Therefore, it represents the main source of blurring for synthetic aperture images [4]. Substituting (5) into (2) yields the motion error affected echo data $\tilde{e}(u, t)$ and consequently, the degraded synthetic aperture image, $\tilde{f}(x_n, y_m)$, is obtained after applying the mapping of (4).

2.2. Image Degradation Model

Autofocus techniques require a degradation model, which relates the focused image to the degraded image by taking into account the characteristics of the imaging mode. Given an appropriate model, the phase error can be estimated and corrected accordingly. While for spotlight operation the same scene is observed for all sensor positions, in stripmap mode each target contains different information about the path deviation function. This is illustrated in Fig. 1(a) and Fig. 1(b) for targets at different along-track and range position, respectively. In the sequel, the blurring model of both operation modes is provided.

Using the narrow-beam approximation as well as the wavenumber transform [1,4]

$$u = y - \frac{k_y}{k_x}(X_c - x),$$

(6)

which relates the spatial along-track frequency k_y to the aperture position u. Using (6), a relationship between the 2-D Fourier transformation of the blurred image and ideal image is provided by

$$\tilde{F}(k_x, k_y) \approx F(k_x, k_y) e^{j k_x x_e \left(y - \frac{k_y}{k_x}(X_c - x) \right)}.$$

(7)

Note that we consider the continuous case here to omit the subscripts for ease of notation. The relation in (7) represents the blurring model for stripmap operation. It illustrates the spatial dependency of the PSF and is only approximate due to a small change in the stationary phase point in the presence of sway errors [4].

In case of spotlight operation, which often assumes a narrow-band system and has a small swath-extent compared to the standoff range, i.e. $X_0, Y_0 \ll X_c$, the wavenumber transform simplifies to

$$u = -\frac{X_c}{2 k_c} k_y,$$

(8)

where k_c is the wavenumber at the carrier frequency [4]. Thus, the relation between aperture position u and along-track wavenumber k_y is simply a scaling factor. Substituting (8) into (7) yields

$$\tilde{F}(k_x, k_y) = F(k_x, k_y) e^{j 2 k_c x_e(k_y)}.$$

(9)

The relation in (9) shows that sway errors cause a blurring in along-track but not in range direction for spotlight modes. As a consequence, spotlight autofocus techniques, e.g. PGA, can be applied and are able to exploit range redundancy.
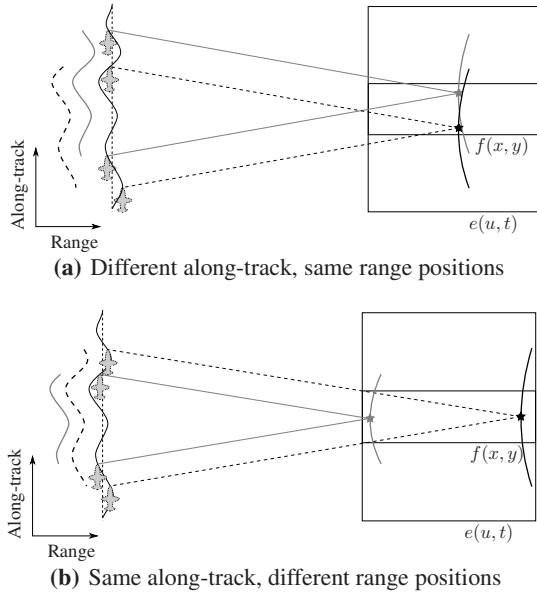

(a) Different along-track, same range positions

(b) Same along-track, different range positions

Fig. 1. Stripmap motion error observed by targets at same range but different along-track positions (a) and same along-track but different range positions (b).

3. AUTOFOCUS

In the sequel, we provide a brief review of the PGA and the mPGA algorithm. For more details, we refer to [2,6].

3.1. Phase Gradient Autofocus (PGA)

The PGA algorithm is a commonly used method to process spotlight SAR images which relies solely on the erroneous image data, $\tilde{f}(x_n, y_m)$, $n = 1, \ldots, N_x$ and $m = 1, \ldots N_y$, and uses the blurring model of (9). It consists of four main processing steps, which are briefly described subsequently.

Circular Shifting
Circular shifting is done in the image domain and starts with the selection of the most dominant scatterer for each range bin x_n, $n = 1, \ldots, N_x$ and circularly shifts them in y-direction to the center of the image. This operation removes the targets' linear phase information, while keeping the phase error information. The circular shifted image is denoted by $\tilde{f}_c(x_n, y_m)$.

Windowing
A central-symmetric window function $w(y_m)$ truncates the circular shifted image: $f_w(x_n, y_m) = f_c(x_n, y_m) \cdot w(y_m)$. This step dismisses the data of weak targets, which act as noise and should not contribute to the phase error estimation.

Thus, only data with the highest SNR is taken into account. The width of the window function is determined based on a pre-defined drop down of the estimated PSF [2].

Phase Gradient Estimation
The estimation of the phase gradient $\Delta\Phi(k_{y_m})$ is the core of PGA and is performed in the along-track wavenumber domain, i.e. $f_w(x_n, k_{y_m})$. The maximum likelihood [2] estimate of the phase error gradient is given by

$$\Delta\Phi(k_{y_m}) = \angle\left(\sum_{n=1}^{N_x} f_w(x_n, k_{y_m}) \cdot f_w(x_n, k_{y_{m-1}})\right),$$

for $m = 2, \ldots, N_y$. The unknown path deviation in the wavenumber domain is then

$$x_e(k_{y_m}) = 1/(2k_c) \sum_{n=1}^{m} \Delta\Phi(k_{y_n}) \text{ with } \Delta\Phi(k_{y_1}) = 0.$$

Iterative Phase Correction
After removing any linear trend, phase correction is performed by multiplying the conjugate of the estimated phase error with $\tilde{f}(x_n, k_{y_m})$. The inverse Fourier transform to the spatial domain yields the phase corrected image of the current iteration. The whole process is repeated until convergence, e.g. the window width does not differ significantly anymore between two consecutive iterations.

3.2. Mosaic Phase Gradient Autofocus (mPGA)

In [6], a method is introduced to apply the standard PGA algorithm to stripmap images by dividing the image into L overlapping along-track stripes. The lth stripe is defined as

$$f_l(x_{n+(l-1)N'}, y_m), \text{ for } n = 1, \ldots, N'_x \qquad (10)$$

where $(l-1)N'$ is the starting point of stripe l and each stripe has a width of N'_x range bins. Choosing a small width, the range-dependency of the phase error within one stripe is negligible and thus, can be assumed to be constant. As a consequence, the spotlight error model can be applied. Each stripe is used as an input for the standard PGA, see Section 3.1, and is focused separately. The new focused image is reassembled by stitching together the individually focused stripes.

4. MODIFIED VERSION OF MOSAIC PHASE GRADIENT AUTOFOCUS

The mPGA accounts for the range dependency of the motion error $x_e(u)$ but it neglects that targets contain different fractions at varying along-track positions as depicted in Fig. 1(a). In this case, the PGA selects the brightest target, shifts it to the center followed by windowing. Thereby, other targets are discarded. Moreover, the estimated phase error is eventually

applied to the entire along-track stripe, ignoring that other targets suffer from different phase errors. This is demonstrated in Fig. 2. Here, the targets selected by the PGA are focused accurately but others in the same stripe are severely blurred and vanish. Another issue related to the mPGA is the inability of the PGA to estimate linear phase errors [3,4]. While a linear phase error induces an entire image shift in along-track for the standard PGA, it may lead to varying along-track shifts for different image stripes causing problems in the reassembling process as shown in Fig. 3. Although the individual stripes are focused correctly, the reassembled image is staggered.

To overcome these drawbacks, we propose a modified version of the mPGA to account for both, the along-track dependency of the error and varying linear shifts for different image stripes. We call the proposed method the modified mosaic Phase Gradient Autofocus (mmPGA) algorithm.
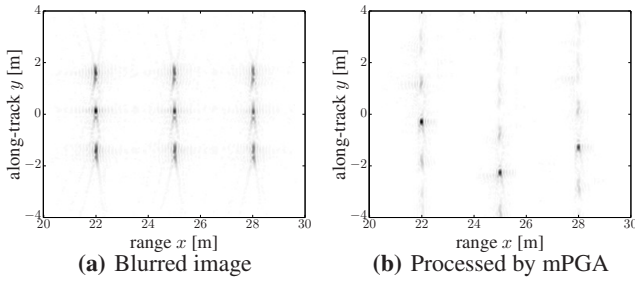

(a) Blurred image   (b) Processed by mPGA

Fig. 2. mPGA focusing issue leading to wrong sway estimates for non-prominent targets displaced in along-track direction.
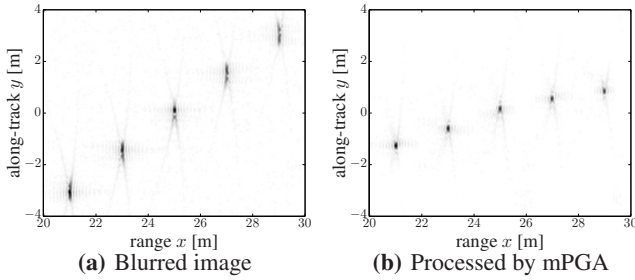

(a) Blurred image   (b) Processed by mPGA

Fig. 3. mPGA focusing issue leading to a staggered image estimate due to varying linear shifts for different image stripes.

4.1. Modifications

First, different along-track positions of targets are considered by dividing the image not only in range but also in along-track direction. Second, the issue of varying linear shifts among image stripes is handled by estimating the individual shifts via correlation of sub-images before and after applying the PGA. The block diagram depicted in Fig. 4 provides an overview of the individual steps of the modified algorithm. The erroneous input image gets decomposed into sub-images $\tilde{f}_{l,k}(x_n, y_m)$. Inside such a "mosaic", it is assumed that every target is exposed to the same section of the motion error. Thus, the phase
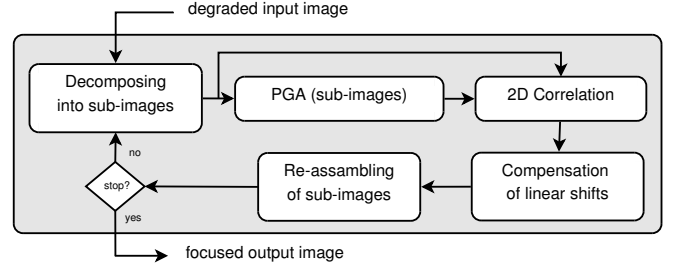

Fig. 4. Block diagram of the proposed modified mPGA

error estimate can be applied to the entire sub-image. To account for varying shifts in individual sub-images, we correlate the input sub-images, $\tilde{f}_{l,k}(x_n, y_m)$, and output sub-images, $\hat{f}_{l,k}(x_n, y_m)$, for each iteration of the PGA to estimate the occurring shifts. The correlation of sub-images (l, k) is estimated by

$$\hat{\rho}_{l,k}(i,j) = \frac{\sum_n \sum_m a_{l,k}(x_n, y_m) b_{l,k}(x_n + i\Delta_x, y_m + j\Delta_y)}{\hat{\sigma}_{l,k}^a \hat{\sigma}_{l,k}^b},$$
(11)

where

$$a_{l,k}(x_n, y_m) = \left| \hat{f}_{l,k}(x_n, y_m) \right| - \hat{\mu}_{l,k}^a$$

and

$$b_{l,k}(x_n, y_m) = \left| \tilde{f}_{l,k}(x_n, y_m) \right| - \hat{\mu}_{l,k}^b$$

are the mean subtracted input and output intensities of the sub-images. The sample mean and sample standard deviation of sub-image (l, k) are denoted as $\hat{\mu}_{l,k}$ and $\hat{\sigma}_{l,k}$, respectively. Moreover, Δ_x represents the pixel size in range direction and Δ_y in along-track direction. Then, the maximum correlation determines the spatial shift between sub-images (l, k) as

$$[i_{\max}, j_{\max}] = \arg\max_{i,j} |\hat{\rho}_{l,k}(i,j)|.$$
(12)

Thus, the linear-shift corrected sub-image (l, k) is given by

$$\hat{f}'_{l,k}(x_n, y_m) = \hat{f}_{l,k}(x_n - i_{\max}\Delta_x, y_m - j_{\max}\Delta_y).$$
(13)

Note that the shift in range $i_{\max}$ typically equals zero since the linear phase error only yields a shift in along-track direction and that we only account for entire pixel shifts. For small correlation coefficients, the estimation of the linear shift is unreliable. Consequently, we only consider shifts for which the correlation coefficient is larger than a certain threshold γ, empirically chosen to be $\gamma > 0.5$. Otherwise, the sub-image is not corrected by the estimated shift. Since this process relies on the blurred image data, the performance is limited by its erroneous along-track information. A linear trend in the motion error $x_e(u)$ can still not be estimated by the algorithm, but rather a linear phase error in the phase estimate of the PGA. The effect of the proposed modifications are illustrated in Fig. 5(b). Compared to Fig. 2(b), significant improvements are visible in the focused image.
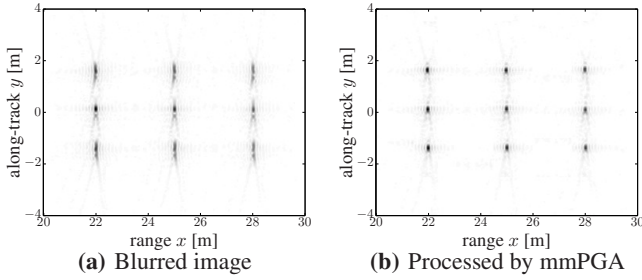
Fig. 5. Modified mPGA applied to a blurred stripmap image

5. SIMULATIONS

The proposed method has been tested using synthetic data generated from $D = 100$ point targets, which have been placed uniformly at random in a scene of interest of size $Y_0 = 3$ m, $X_0 = 5$ m and $X_c = 25$ m. A sinusoidal path deviation function with an amplitude $A = 0.1\lambda_c$, where λ_c is the wavelength at the carrier frequency, and a cycle per synthetic aperture length frequency of $\nu = 2$ has been set to deteriorate the reconstruction. A total number of $M = 100$ experiments have been conducted. Fig. 6(a)-(d) show exam-
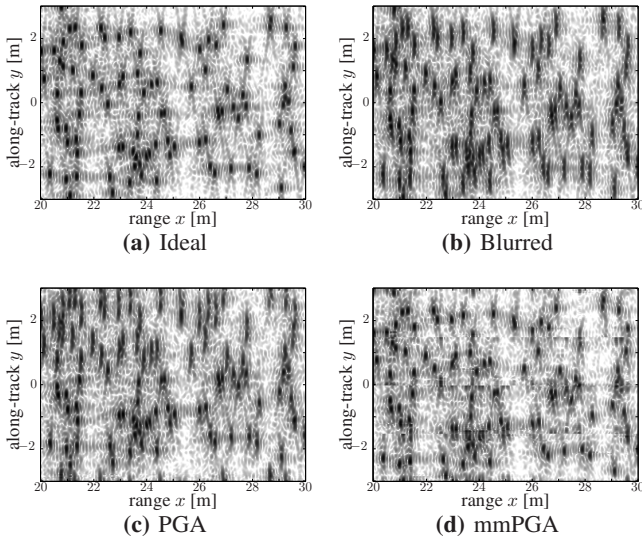

Fig. 6. Illustration of a focusing example showing the ideal reconstruction of the target scene (a), the blurred image (b) and the images after applying the PGA (c) and mmPGA (d).

ple results of the ideal reconstructed image in Fig. 6(a), the blurred image in Fig. 6(b), and the autofocused images using the PGA in Fig. 6(c) and the proposed method, mmPGA, in Fig. 6(d). All figures are shown with a dynamic range of 40 dB. Note that the mPGA is not depicted since it has shown poor performance due to the issues addressed in Section 4. While the PGA focuses some of the scatterers in the lower region of the image, the mmPGA is capable to focus the entire scene. However, it introduces some blocking artifacts. In or-

der to evaluate the simulation results, the structural similarity index (SSIM) [7] as a full reference image quality measure has been applied. Note that each image has been registered with respect to the ideal image before applying the metric. The outcome is depicted in Fig. 7 for $N_{iter} = 10$ fixed iterations for each autofocus technique. Iteration $q = 0$ provides the SSIM of the blurred image. The curves show the failure of the PGA and mPGA, which both degrade the blurred image significantly during the first iteration and then rapidly converge to a low SSIM value. Contrarily, the mmPGA improves the image quality in the first iteration and then converges. The latter is important to be able to apply flexible stopping criteria.
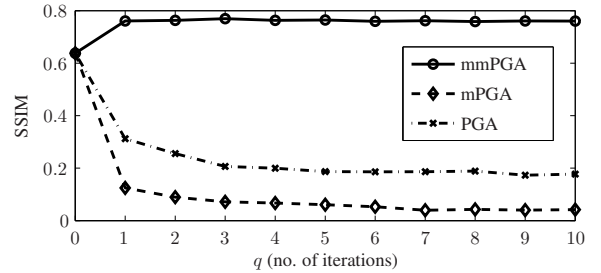

Fig. 7. SSIM evaluation of autofocus techniques $N_{iter} = 10$ iterations. $q = 0$ shows the SSIM of the blurred image.

6. CONCLUSION

We have introduced a modified version of the mPGA algorithm to overcome its shortcomings when focusing stripmap synthetic aperture imagery. The validity of the proposed method has been proven using simulations with synthetic data. As a next step, we will adapt the method to lower the blocking effects and apply it to real stripmap SAS images.

7. REFERENCES

[1] M. Soumekh, *Synthetic aperture radar signal processing with MATLAB algorithms*, Wiley & Sons, 1999.

[2] D. E. Wahl, P. H. Eichel, D. C. Ghiglia, and Jr. Jakowatz, C. V., "Phase Gradient Autofocus-A Robust Tool for High Resolution SAR Phase Correction," *IEEE Transactions on Aerospace and Electronic Systems*, vol. 30, no. 3, pp. 827–835, 1994.

[3] D. E. Wahl, Jr. Jakowatz, C. V., P. A. Thompson, and D. C. Ghiglia, "New Approach to Strip-Map SAR Autofocus," in *Proc. Sixth IEEE Digital Signal Processing Workshop*, 1994, pp. 53–56.

[4] Hayden J. Callow, *Signal Processing for Synthetic Aperture Sonar Image Enhancement*, Ph.D. thesis, University of Canterbury, Christchurch, New Zealand, April 2003.

[5] H. J. Callow, M. P. Hayes, and P. T. Gough, "Strip-map Phase Gradient Autofocus," in *Proc. OCEANS 2003*, 2003, vol. 5, pp. 2414–2421.

[6] W. W. Bonifant, Jr., "Interferometic Synthetic Aperture Sonar Processing," Master's thesis, Georgia Institute of Technology, July 1999.

[7] Zhou Wang, A. C. Bovik, H. R. Sheikh, and E. P. Simoncelli, "Image Quality Assessment: From Error Visibility to Structural Similarity," *IEEE Transactions on Image Processing*, vol. 13, no. 4, pp. 600–612, 2004.